

Optical Engineering

OpticalEngineering.SPIEDigitalLibrary.org

Direct design approach to calculate a two-surface lens with an entrance pupil for application in wide field-of-view imaging

Yunfeng Nie
Fabian Duerr
Hugo Thienpont

Direct design approach to calculate a two-surface lens with an entrance pupil for application in wide field-of-view imaging

Yunfeng Nie,* Fabian Duerr, and Hugo Thienpont

Vrije Universiteit Brussel, Brussels Photonics Team, Department of Applied Physics and Photonics, Pleinlaan 2, Brussels B-1050, Belgium

Abstract. In this work, a multifields optical design method aiming to calculate two high-order aspheric lens profiles with an embedded entrance pupil is proposed. This direct design algorithm is capable of partially coupling more than three ray bundles that enter the same pupil with only two surfaces. Both infinite and finite conjugate objectives can be designed with this approach. Additional constraints such as surface continuity and smoothness are taken into account to calculate smooth and accurate surface contours described by point clouds. The calculated points are then fitted with rotationally symmetric functions commonly used in optical design tools. A presented subaperture sampling strategy that introduces a weighting function for different fields allows for a very well-balanced imaging performance over a wide field of view (FOV). As an example, a ± 45 deg $f/7.5$ wide-angle objective is designed and analyzed to demonstrate the potential of this design method. It provides an excellent starting point for further optimization of the surfaces' coefficients and initial design parameters, resulting in a very good and well-balanced imaging performance over the entire FOV. © The Authors. Published by SPIE under a Creative Commons Attribution 3.0 Unported License. Distribution or reproduction of this work in whole or in part requires full attribution of the original publication, including its DOI. [DOI: [10.1117/1.OE.54.1.015102](https://doi.org/10.1117/1.OE.54.1.015102)]

Keywords: geometric optics; imaging; optical design; lenses; aspherics; optical systems.

Paper 141634 received Oct. 22, 2014; accepted for publication Dec. 9, 2014; published online Jan. 12, 2015.

1 Introduction

Free-form optics has prospered in recent decades with the development of high precision single-point diamond turning and mass replication technology. The advent of free-form optics is more than an evolution for optical engineers due to its unprecedented power in controlling the paths of light rays.¹ More specifically, it provides great potential for correcting optical aberrations in imaging systems,² such as distortion^{3–5} or astigmatism.^{6,7}

Free-form optical systems are typically either designed by multiparametric optimization techniques^{2,5,7–12} or using a direct design method.^{3,4,6,13–16} Multiparametric optimization techniques are widely used to design optical systems. Common procedures are to start from Seidel aberration theory and apply it to solve an initial approximate optical system design, or to use a related already existing optical system design to start from. Then the parameters describing the optical system are varied using an optimizer to find better solutions according to a specified merit function. As a free-form surface description can contain many more parameters than “conventional” spherical or conic surfaces, the multiparametric optimization design approach can encounter problems in designing free-form optics: the speed of convergence may be slow; the optimizer is likely to reach a local minimum and not be effective in finding a global minimum; the performance of the optical design does not improve when the number of optimization parameters is increased, because the aspheric coefficients of one surface are cancelling those of another surface.¹⁷ In contrast, direct design methods allow calculating unconstrained optical surfaces (which means

virtually any shape is possible) to fulfill certain imposed requirements.

As a pioneering direct optical design approach, the simultaneous multiple surface design method (SMS) has been steadily developed from utilizing a single surface to more than six surfaces.^{13,18–20} It allows perfect coupling of rays from two fields into two image points by using two surfaces. Recently, it has been shown by Duerr et al. that in certain cases, it is possible to couple three ray bundles with only two lens surfaces.²¹ Besides an ideal imaging performance for the designed fields, both design approaches still show very good imaging performance for moderate deviations from the chosen fields. However, with an increasing field of view (FOV), additional in-between fields should be considered in the design approach to maintain a well-balanced imaging performance over the entire FOV. Furthermore, most existing direct design approaches have not yet incorporated a pupil in the design process. Few direct designs that include a pupil exist: a single surface design as the interface between two media by Liu,⁶ Hou⁴ and Zhu¹⁶ also utilized an entrance pupil in their two lens surfaces design. However, in Hou's work, only three rays of one specific field are considered and the fields are discretely and separately designed, which introduces restrictions by making the tangent of the marginal rays in two neighboring fields identical. In Zhu's work, only the first lens profile is directly calculated, whereas the second lens profile is still obtained by optimization.

In this work, we propose a new direct design approach that partially couples multiple unconstrained fields with two lens profiles, including an entrance pupil to make the marginal rays easier to control. Essential prerequisites for such a system to work properly are discussed and explained in detail in Sec. 2. In Sec. 3, a lens with a ± 45 deg FOV is designed to demonstrate the functionality of the proposed

*Address all correspondence to: Yunfeng Nie, E-mail: ynie@b-phot.org

design method. A subaperture balancing strategy, which enables a very well-balanced imaging performance over the entire FOV, is presented in Sec. 4. In Sec. 5, the calculated two-dimensional (2-D) lens profiles are used to design a rotationally symmetric system in combination with a spherically front negative lens to serve as a two-lens wide-angle objective. The ray tracing evaluation in terms of root mean square (RMS) spot diameters shows excellent imaging performance when compared to a conventional wide-angle objective using four spherical lenses. Finally, in Sec. 6, conclusions are drawn and an outlook is given.

2 Initial Degrees of Freedom and Prerequisites for Direct Lens Design with a Pupil

A realistic imaging system consists of an object, a pupil, an optical system, and a detector schematically shown in Fig. 1(a). In this first case, the two lens surfaces are largely covered by the two ray bundles, leaving little “free space” for coupling additional ray bundles of other in-between fields. The position of the pupil plays an important role in correcting off-axis aberrations, especially coma.²² In most existed direct design cases,^{15,23,24} the entrance pupil is also the first optical surface of the system, neglecting the function of an independent pupil in diminishing optical aberrations.

In Figs. 1(b) to 1(d), the overlapping regions on the lens profiles of two or more different ray bundles become smaller and smaller and might eventually vanish by increasing the pupil distance from the first lens surface and/or reducing the pupil aperture size. This restricted overlapping of different ray bundles on the lens surfaces due to a shifted pupil position provides sufficient degrees of freedom to couple an on-axis ray bundle at least partially, as shown in Fig. 1(c).

If we continue enlarging the pupil distance and shrinking the pupil aperture further, five or more ray bundles can be perfectly coupled with two surfaces, illustrated in Fig. 1(d). This qualitative description provides a comprehensive explanation of the impact of the pupil for direct optical designs. It allows coupling more ray bundles than the number of optical surfaces either completely or at least partially.

One possible design strategy could be as follows: each ray bundle occupies an isolated portion of the lens described by a Cartesian oval; these Cartesian ovals for different fields are then connected together to form a full 2-D lens. There might be some remaining gaps in the second lens profile, and the smoothness at the connection points between different fields in the first lens profile needs to be adjusted. Furthermore, the two lens profiles then locally couple only a single ray bundle instead of the possible two ray bundles simultaneously.

Three prerequisites are identified to overcome the problems listed above:

1. Each part of each lens profile couples two discrete fields to maximize the utilization of the degrees of freedom of both profiles.
2. The segments created by adjacent fields should intersect or overlap to avoid gaps which can result in wavefront aberrations and potential discontinuity.
3. The smoothness of the overall lens profiles at the connection points between different fields is guaranteed by implementing an appropriate optical path lengths (OPLs) relationship between different fields. However, the OPLs for different ray bundles cannot be calculated and need to be found by optimization, see for example Ref. 25.

3 Design Algorithm of a Two-Surface Lens Coupling Multifields with a Pupil

The presented design approach aims to fulfill the prerequisites explained in Sec. 2. The two lens profiles being designed are divided into several sections, where each section couples rays simultaneously emitted from two different fields. An angle increment θ is introduced to guarantee that the chief ray of a new field intersects with already known segments of both surfaces, which is necessary for calculating the corresponding otherwise unknown OPL. All OPLs of different off-axis fields will be directly determined in advance by calculating the trajectories of corresponding chief rays

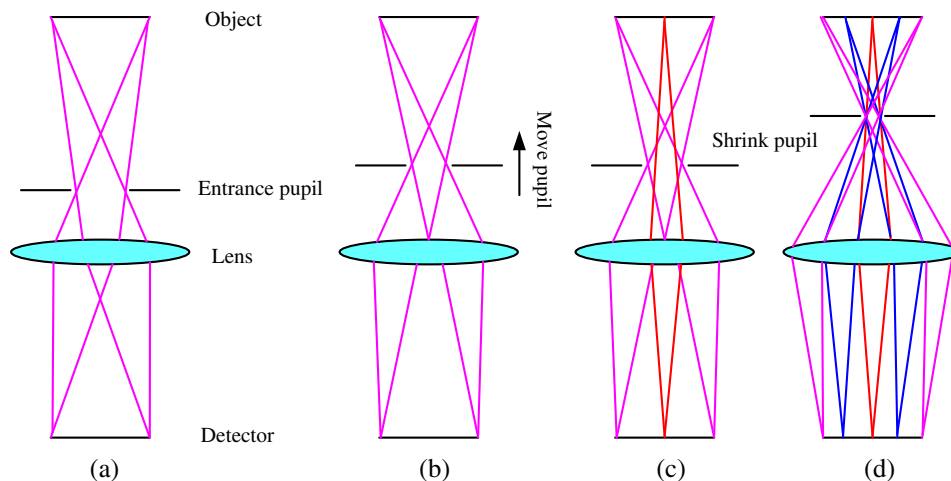


Fig. 1 (a) Geometry of a simplified optical system with a pupil and its selection of marginal ray bundles. (b) The overlapping region of the two ray bundles becomes smaller by moving the entrance pupil away from the lens. (c) A portion of rays from the on-axis field can be coupled as a result. (d) By further enlarging and shrinking the entrance pupil, it is possible to perfectly couple five fields (or even more) with only two optical surfaces.

during the design process. The complete design procedure consists of five steps:

- (1) As shown in Fig. 2(a), the algorithm starts with a central on-axis ray along the optical axis, passing through points E_0, M_1, N_1, R_0 and an initial segment M_1M_2 . Generally, the initial segment can be represented by an even-order polynomial to satisfy the symmetry of the surface, for example a second-order form

$$y = ax^2 + b. \tag{1}$$

After choosing these initial points, the central thickness of the lens and the positions of the object and image planes are determined. Both normal vectors of points M_1 and N_1 are in the direction of the optical axis due to the overall symmetry of the lens. Points P_1 and P_2 define the position of the entrance pupil and its diameter. The segment N_1N_2 is calculated by sampling a considerable number of points on

the seed segment M_1M_2 and then tracing rays between E_0R_0 keeping a constant OPL. The initial calculation of segments M_1M_2 and N_1N_2 guarantees the construction of new OPLs for off-axis chief rays.

- (2) Given that subsequent calculation of the two lens profiles will simultaneously proceed between two ray bundles, at least two new OPLs should be determined in advance to ensure the process. Therefore, two new off-axis chief rays are gradually picked by increasing the incident chief ray angle θ in addition to the chief ray of the previous field, shown in Figs. 2(b) and 2(c). The value of θ is constant and constrained to guarantee that at least two off-axis chief rays intersect with the already known initial lens profiles. Since the trajectories of these two chief rays are determined, their corresponding OPLs are directly calculated without introducing additional variables. In addition, two new points N_3 and N_4 on the second profile are calculated by applying the constant OPL condition, and

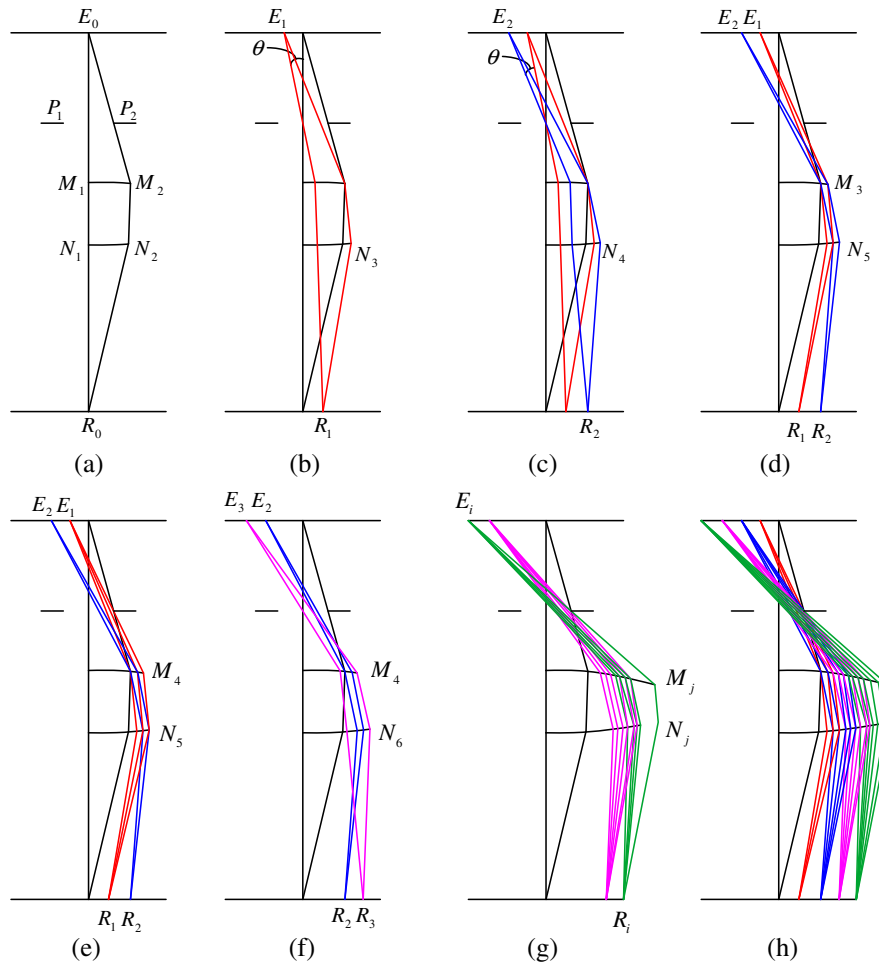


Fig. 2 Illustration of the design procedure to calculate two lens profiles partially coupling N ($N > 3$) ray bundles. (a) The chosen initial parameters determine the central lens thickness and the first optical path lengths (OPL). (b) and (c) Two new initial OPLs for two off-axis fields E_1, E_2 by an increment of the incident chief ray angle θ and the corresponding new points N_3, N_4 are calculated. (d) and (e) Both lens profiles are simultaneously calculated by applying constant OPL condition between two off-axis fields until reaching a stop criterion. (f) Repeated procedure for a new field E_3 . (g) and (h) The lens profiles for the maximum field are finalized by interpolating known points and extending into the full aperture.

their corresponding normal vectors are calculated by applying Snell's law.

- (3) In Fig. 2(d), the design process continues by tracing a ray from image point R_1 propagating through N_4 which results in a new point M_3 on the first profile. Next, a ray is emitted from E_2 to calculate a new point N_5 by utilizing the constant OPL condition. Following the process, new points on the first and second profiles are calculated between fields E_1 and E_2 by turns until the full pupil aperture for one of the two fields is reached (indicated by the point M_4), as shown in Fig. 2(e).
- (4) The lens profiles are further repeatedly extended by calculating new OPLs and tracing rays between two adjacent fields. Similarly to step (2), a new field E_3 is created with an increment angle θ and a predetermined OPL, shown in Fig. 2(f). Point N_6 is calculated by a ray emitted from E_3 going through point M_4 , allowing a repetition of the design process of step (3).

In this step, the value of θ is further constrained to guarantee that the new chief ray intersects with a known part of the lens profile. As shown in Fig. 3, the first profile is approximately considered to be flat. X_0 is the length of the initial segment and M_2 indicates the already known lens profile after step (3). L and L_1 are, respectively, the object distance and pupil distance from the lens, D is the diameter of the pupil. Conditions are satisfied if the lens profile increases faster than the intersection point of the new chief ray on the thin lens. Therefore, the constraints that θ should obey are as follows:

$$L_1 \cdot \tan 2\theta \leq X_0, \tag{2}$$

$$L_1 \cdot \tan 2\theta \leq \frac{D}{2} \cdot \frac{L}{L - L_1}. \tag{3}$$

- (5) Step (4) is repeated until reaching a maximum specified field angle. To finalize the last part of the lens, a final curve is defined as a third-order polynomial. As at least two points on the first profile for the maximum field are known and this last lens segment can be determined by interpolating the first and

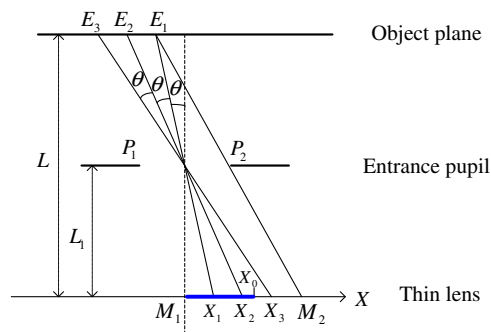


Fig. 3 The first two OPLs are created when $X_2 \leq X_0$ (The length of the initial segment). New chief ray E_3X_3 intersects with known lens profiles when the lens profile increment X_1M_2 is larger than the distance X_1X_3 .

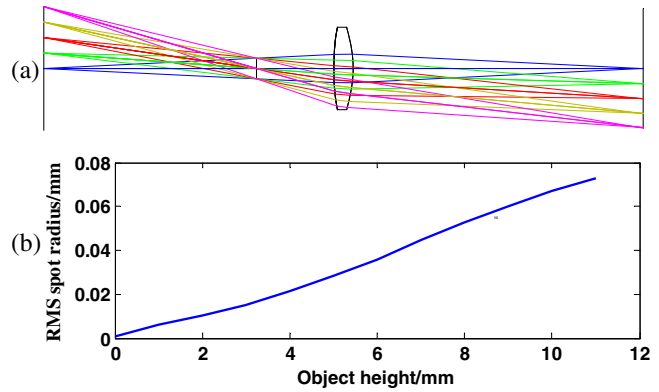


Fig. 4 (a) The architecture of a two-dimensional (2-D) lens designed by multifields method with a pupil aperture 4 mm and (b) its root mean square (RMS) spot radius performance starts from an excellent on-axis quality ($0.8 \mu\text{m}$) and nearly linearly decreases to the worst at the maximum object height ($78 \mu\text{m}$).

last of the already known points and their normals. This final curve element is then extended to intersect with the marginal ray E_iM_i , as shown in Fig. 2(g). By sampling rays emitted from the maximum field to cover the full aperture, the last portion of the second profile is calculated using a constant OPL condition. The final design result is displayed in Fig. 2(h).

A monochromatic exemplary design with a pupil aperture of 4 mm is calculated using this design approach, as shown in Fig. 4(a). The object and image planes are both 60 mm away from the lens with both diameters of 23 mm, and the thickness of the lens is 4 mm. The distance from the entrance pupil to the lens is 16 mm. Compared to the design strategy where discrete ray bundles are perfectly coupled in Sec. 2, the subsequent approach has the advantage that the surfaces are smooth without any further optimization process of various OPLs for different fields. Although not all rays are sampled for each field, the method already achieves a good imaging performance in terms of RMS spot radius, as shown in Fig. 4(b). While the on-axis field is perfectly coupled by this lens (revealed by the RMS spot radius $0.8 \mu\text{m}$), the RMS spot radius almost linearly increases from on-axis to the maximum field: far from being well balanced over the entire FOV.

4 Balancing Multifields Performance by Adjusting Virtual Subaperture Factors

When designing any imaging lens, a well-balanced imaging performance among different fields is typically required. To balance the image quality over the entire FOV, our multifields balancing strategy works as follows: by using the multifields design method of Sec. 3, only a portion of the ray bundles passing through the full pupil is now selected, similar to adding a "vignette factor." By adjusting the "vignette factor" of each field, the level of partial perfect coupling of all ray bundles can be controlled, targeting a more balanced image quality. The idea of a virtual subaperture is illustrated in Fig. 5.

As shown in Fig. 5(a), given a single lens system with a relatively large pupil aperture, the on-axis field determines already a large portion of both lens profiles, as the initial segment explained in Sec. 3. Such a large aperture makes the

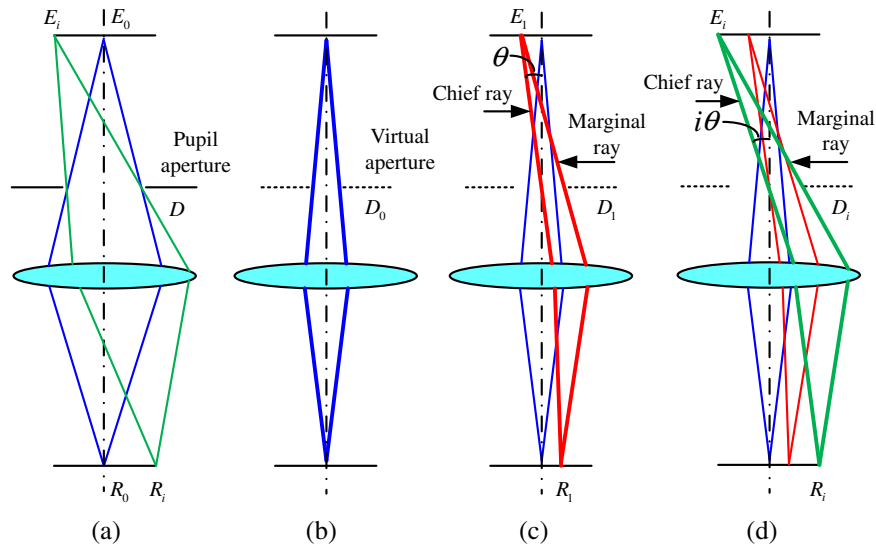


Fig. 5 (a) A single lens system with relatively large pupil aperture where initial segment occupies most of the lens profiles. (b) A virtual aperture is introduced to shrink initial segment. (c) and (d) The lens profiles coupled by other fields are thereby more balanced.

subsequent design steps less powerful to partially couple multiple fields. In order to reduce the impact of the initial segment on the design process, a virtual smaller aperture is incorporated to reduce the size and the impact of the initial segment, as shown in Fig. 5(b). The bold light rays in Figs. 5(b) to 5(d) highlight the lens segments determined by different fields. By adjusting the size of the virtual aperture for each field, a balanced segment distribution of different fields is achieved, as shown in Fig. 5(d).

We can define a subaperture factor $W_i = D_i/D$ (the “vignette factor”) for each field. D_i denotes the diameter of the virtual aperture for a certain field i , and D is the diameter of the full entrance pupil. These subaperture factors indicate the proportion of the ray bundles being sampled for certain fields and determine the marginal ray for the stop criterion.

In the original approach of Sec. 3, the subaperture factors are 1 for all fields. Given that the on-axis field determines most of the two lens profiles, decreasing the on-axis subaperture factor will enlarge the “free” parts of the lens profiles

for other fields. Suppose the aperture diameter is standardized to 1, then we define three subaperture factors for on-axis, half, and full field separately. The fields between on-axis and half field as well as those between half and full field are assigned to two further subaperture factors, which make five factors in total. This arrangement of subaperture factors gives an opportunity to emphasize both 0.5 and 1 fields as well as to alleviate the importance of the on-axis field.

The RMS spot radius sizes of different designs for different subaperture weighting factor distributions are shown in Fig. 6. The best of them is obtained by a manually controlled feed-back approach. First, the factor of the maximum field should be kept 1 to make the aperture fully sampled without vignetting. By narrowing the virtual aperture factors of all the other fields from 1 to 0.5 and finally 0.25, the whole image quality is greatly improved. However, the RMS spot radii of the second half fields are still not as good as the first half. Therefore, we slightly increased the factor of 0.5 field from 0.25 to 0.5 and finally 0.8 where we have achieved a very good and well-balanced performance among all the fields. The comparison of different distributions also demonstrates that controlling rays from the 0.5 field has a larger impact than its adjacent fields. This strategy is similar to what is done in optimization-based optical design where weighting factors are used to balance the performance of certain specified fields such as the 0.5 and 0.7 fields.

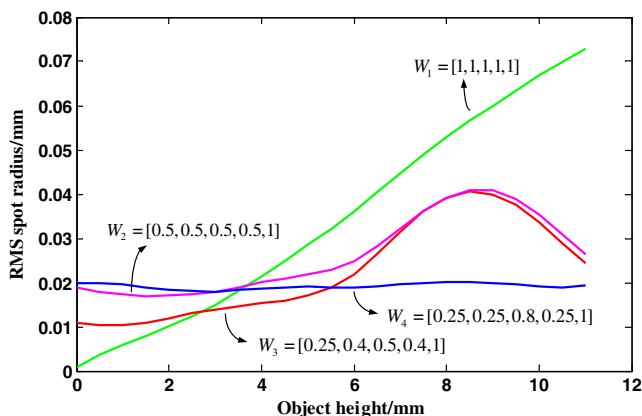


Fig. 6 The comparison of the obtained RMS spot radii for various different weighting function distributions W_i shows that it is possible to achieve a very good and well-balanced performance among all the different fields, which is the case of distribution W_4 .

5 Design Example for a Compact Wide-Angle Infinite Conjugate Objective Lens

As a practical example, a wide angle infinite conjugate object is designed in this section using the proposed approach as a starting point for further optimization.

5.1 Calculation of the Initial Point Clouds by Using the Multifields Method

Wide-angle objective lenses are popular with architectural, interior, and landscape imaging where the photographer may not be able to move farther from the scene to allow

Table 1 Specifications of a wide-angle objective.

Wavelength	Focal length	Field of view	Back focal length	Entrance pupil
550 nm	30 mm	±45 deg	≥ 30 mm	4 mm

more of the scene to be included. One difficulty of designing a wide-angle lens is to maintain a long back focal length (BFL) (at least longer than the focal length), which is desirable for the instruments that need long working distances, for example for single-lens reflex cameras. Such a wide-angle objective will be designed for the specifications listed in Table 1.

In infinite conjugate imaging situations, the incident light rays are regarded as plane wave fronts. The proposed multifields algorithm can be modified to accommodate with the infinite objects by defining plane wave fronts substituting the former object points. The refractive index of the single lens is 1.5, but could be any value of typically used glass or plastic. The whole ±45 deg FOV is divided into 91 fields by a $\theta = 1$ deg chief ray increment during the design process. A central thickness of 4 mm is chosen to guarantee a large enough edge thickness. After choosing these initial parameters, the only remaining variable is the shape factor a of the initial segment. To make the incident angle as small as possible, a positive a in Eq. (1) is preferred (here, the positive a corresponds to a concave front surface).

The subaperture factors are also optimized by using the multifields balancing strategy explained in Sec. 4. An even performance has been achieved for the weighting distribution $W_i = [0.3, 0.4, 0.6, 0.4, 1]$, close to the best distribution of subaperture factors for the finite object design in Sec. 4.

5.2 Two-Dimensional Optimization Using the Optical Software Zemax

After the implementation of the design procedure, the two lens profiles are described by point clouds, which cannot be directly used for ray tracing in Zemax. Since most optical design tools use mathematical expressions to describe optical surfaces, the point clouds need to be transformed first.

Three different expressions typically used to characterize high-order rotationally symmetric aspheric surfaces have been compared: the extended aspheric polynomials, Forbes Q-con,²⁶ and Q-bfs polynomials.²⁷ All of them can achieve sufficient accuracy with the same orders (sixth in this case). Q-con polynomials have been used for the surface fitting in this design. The general expression for Q-con polynomials is given in Ref. 26:

$$z(\rho) = \frac{c\rho^2}{1 + \sqrt{1 - (1 + K)c^2\rho^2}} + \left(\frac{\rho}{\rho_{\max}}\right)^4 \sum_{m=0}^M a_m Q_m^{\text{con}} \left[\left(\frac{\rho}{\rho_{\max}}\right)^2\right], \quad (4)$$

where c is the paraxial curvature of the surface and K denotes the conic constant. We have used sixth-order Q-con polynomials to fit the rotationally symmetric lens surfaces.

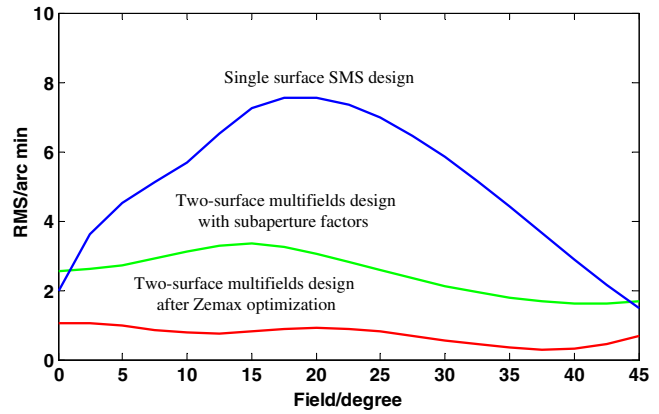


Fig. 7 The single surface simultaneous multiple surface (SMS) design of Ref. 6 provides good imaging performance at the design angles 0 deg and ±45 deg. The two-surface multifields design method achieves a good and well-balanced image quality over the entire design angle range from 0 deg to ±45 deg. Its imaging performance is even further improved after optimization in Zemax.

The best fitting results are given by the following values for the front surface: radius is -60.011 mm, the sixth-order Q-con coefficients are [1.199, 1.898E - 003, 0.041, 0.036, 0.013, and 9.329E - 003]; and for the rear surface: radius is -12.095 mm, the sixth-order Q-con coefficients are [1.821, 0.256, -0.021, 5.621E - 003, -2.354E - 003, -1.957E - 003]. The optimization in Zemax for all initial design parameters (10 fields between 0 and 45 deg, monochromatic wavelength at 550 nm) quickly obtained a better performance by varying the surfaces' parameters and the distances.

Both the performance before and after optimization in Zemax by the multifields design method are evaluated for a 2-D angular RMS spot radius, which is the angular size of RMS spot radius normalized by the distance of corresponding image point to the entrance pupil center. In this way, it is possible to compare the result with the single surface design by the SMS method presented in Ref. 6.

As shown in Fig. 7, the single surface SMS design has a good performance of inner and outer fields, while the multifields method balances the performances of all the fields very well. The result with the multifields design method is further improved after the multiparameter optimization of Zemax.

5.3 Three-Dimensional Wide Field-of-View Objective Design

Although the proposed multifields design method is currently only a 2-D method, the calculated lens profiles can be used as the starting point for the optimization of three-dimensional (3-D) rotationally symmetric lenses. The entrance pupil is modified from a 2-D slit to a standard circular aperture. In order to cover a wide-angle FOV, it is very common to use a strong negatively powered front element or group of elements to bend the rays outward.²⁸ Therefore, one additional negative spherical lens is added in front of the calculated lens to allow rays from wide-angle fields, as shown in Fig. 8(b). Figure 8(a) shows an all-spherical wide-angle objective design. Each of them is designed to be a ±45 deg $f/7.5$ objective with a 30-mm focal length.

Both the conventional all-spherical design and the two lenses system designed by the proposed method have been optimized in Zemax. We have used the default error

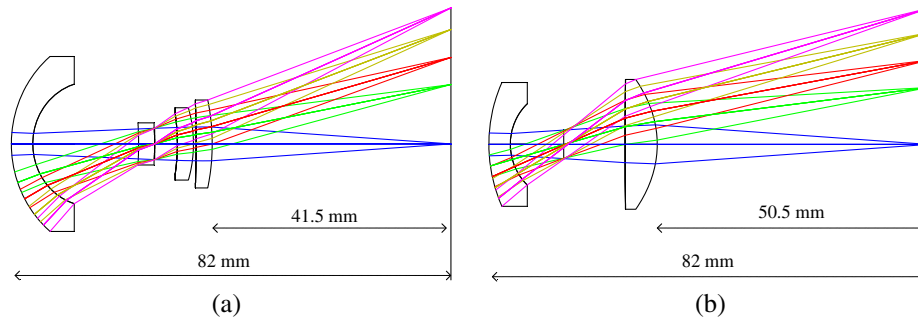


Fig. 8 Two ± 45 deg $f/7.5$ wide-angle objectives with 30-mm focal length. (a) A conventional design with four spherical lenses (modification of US patent No. 4333714 for monochromatic application). (b) The architecture in combination of a negative spherical front lens (first no power and then optimized into its final shape) and a calculated rear lens designed by multifields method in Sec. 5.1.

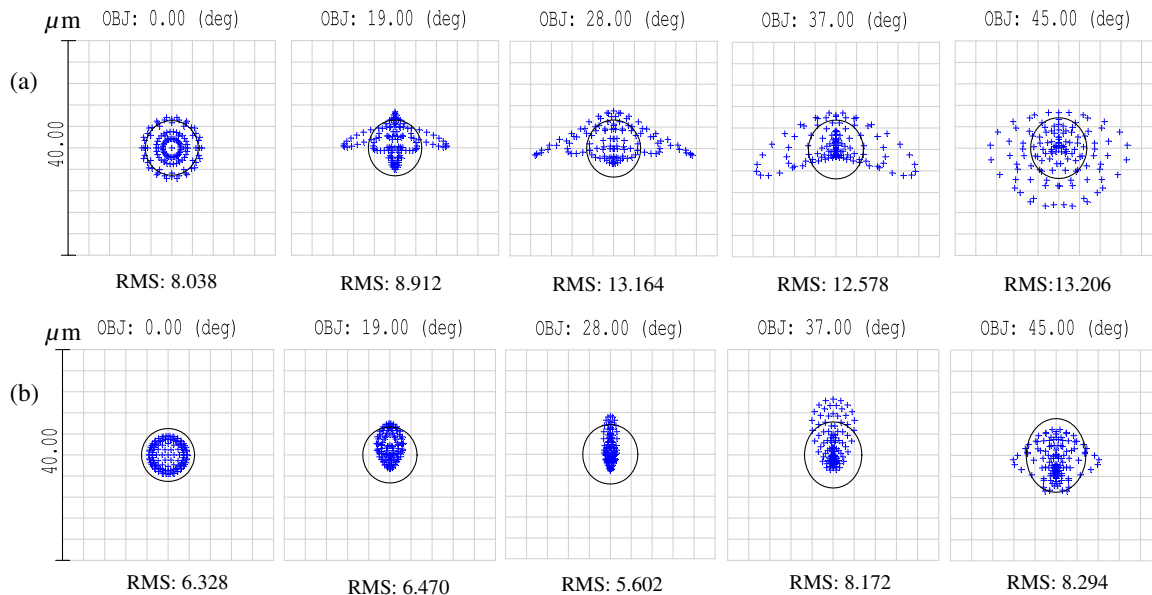


Fig. 9 The direct comparison of the spot diagrams for a conventional all-spherical design (a) and the multifields design combined with a spherical lens (b) clearly shows better performance for the combination design method.

function of Zemax in both cases by evaluating the RMS of spot radii for the selected five fields (0, 19, 28, 37 and 45 deg). The chief ray of each field is selected as a reference; the error function is then built by calculating the RMS of the deviations of the sampled rays on the image plane. Two additional operands are added to control the effective focal length and the overall length.

The 2-D layout of the optimized design results is shown in Fig. 8 with the same scale. The distortion is not corrected in either case; each of them is about 20%. The result based on the multifields design method is more compact than the all-spherical design; it only consists of two optical elements while the latter consists of four, and the total lengths of the two designs are both 82 mm while the former has a longer BFL.

In order to compare the image quality of both designs, the RMS spot diameters are evaluated and shown in Fig. 9. The wide-angle objective designed with the multifields method and further optimized demonstrates a clearly better overall performance when compared with its all-spherical lenses counterpart. The added black circles in the spot diagrams

correspond to the airy disk diameters (determined from real ray tracing) at the reference wavelength and f-number. The RMS spot diameter values range from 5.6 to 8.3 μm in the combination design, compared with 8 to 13.2 μm in case of the all-spherical lens design for the identical incident angle range [0 deg, ± 45 deg].

This result clearly emphasizes the potential of such a combined strategy: using the multifields direct design method to derive an excellent starting point which is then further optimized to achieve more compact well-performing optical systems.

6 Conclusion

Within the scope of this work, a new multifields direct design method has been presented. This method allows us to simultaneously calculate two lens profiles that partially couple multiple fields with an incorporated entrance pupil. Including an entrance pupil in the design process is key to gaining control of multiple fields with only two optical surfaces.

To satisfy the identified prerequisites, a strategy to precalculate new OPLs of different fields is proposed; it not only guarantees the smoothness of surfaces, but also allows the calculation of new points to further extend both lens profiles. The presented idea of independently introducing a set of subaperture “vignette” factors provides the flexibility to choose the degree of coupling for each off-axis field. By adjusting the subaperture factor distribution, it is possible to achieve a very good and well-balanced imaging performance over a wide FOV.

The potential of this new design approach has been successfully demonstrated for the optical design of a wide-angle objective with a ± 45 deg FOV. In combination with a negative spherical front lens for covering wide-angle rays, this design enables not only a more compact structure but also achieves a better imaging performance in terms of RMS spot diameters when compared with its all-spherical counterpart.

Future work will focus on the extension of this design strategy for 3-D free-form surfaces regarding imaging applications with high aspect ratios.

Acknowledgments

The work reported in this paper is supported in part by the People Programme (Marie Curie Actions) of the European Union’s Seventh Framework Programme (FP7/2007-2013) under REA Grant Agreement No. PITN-GA-2013-608082 (ADOPSYS), by the Research Foundation—Flanders (FWO-Vlaanderen) that provides a postdoctoral grant to Fabian Duerr, and in part by the IAPBELSPO grant IAP P7-35 photonics@be, the Industrial Research Funding (IOF), Methusalem, and the OZR of the Vrije Universiteit Brussel.

References

1. J. Rolland and K. Thompson, “Freeform optics: evolution? No, revolution!” *SPIE Newsroom* (2012).
2. K. Fuerschbach, J. P. Rolland, and K. P. Thompson, “A new family of optical systems employing ϕ -polynomial surfaces,” *Opt. Express* **19**(22), 21919 (2011).
3. R. A. Hicks, “Direct methods for freeform surface design,” *Proc. SPIE* **6668**, 666802 (2007).
4. J. Hou et al., “Method to design two aspheric surfaces for imaging system,” *Appl. Opt.* **52**(11), 2294 (2013).
5. B. Yang et al., “Free-form lens design for wide-angle imaging with an equidistance projection scheme,” *Optik—Int. J. Light Electron Opt.* **120**(2), 74–78 (2009).
6. J. Liu et al., “Single optical surface imaging designs with unconstrained object to image mapping,” *Proc. SPIE* **8550**, 855011 (2012).
7. T. Ma et al., “Design of a freeform varifocal panoramic optical system with specified annular center of field of view,” *Opt. Express* **19**(5), 3843 (2011).
8. O. Cakmakci et al., “Design of a free-form single-element head-worn display,” *Proc. SPIE* **7618**, 761803 (2010).
9. K. Takahashi, “Development of ultrawide-angle compact camera using free-form optics,” *Opt. Rev.* **18**(1), 55–59 (2011).
10. L. Li and A. Y. Yi, “Design and fabrication of a freeform microlens array for a compact large-field-of-view compound-eye camera,” *Appl. Opt.* **51**(12), 1843–1852 (2012).
11. J. Sun et al., “Study of extended optimization for U-type 2 \times zoom optics with free-form surface,” *Opt. Laser Eng.* **48**(3), 368–379 (2010).
12. D. Cheng et al., “Design of an optical see-through head-mounted display with a low f-number and large field of view using a freeform prism,” *Appl. Opt.* **48**(14), 2655–2668 (2009).
13. J. C. Minano et al., “An application of the SMS method for imaging designs,” *Opt. Express* **17**(26), 24036–24044 (2009).
14. A. M. Herkommer, “Phase space optics: an alternate approach to free-form optical systems,” *Opt. Eng.* **53**(3), 031304 (2014).
15. F. Duerr et al., “Analytic design method for optimal imaging: coupling three ray sets using two free-form lens profiles,” *Opt. Express* **20**(5), 5576–5585 (2012).
16. J. Zhu, T. Yang, and G. Jin, “Design method of surface contour for a freeform lens with wide linear field-of-view,” *Opt. Express* **21**(22), 26080 (2013).
17. R. E. Fischer et al., *Optical System Design*, McGraw Hill, New York (2000).
18. P. Benítez and J. C. Miñano, “Simultaneous multiple surface optical design method in three dimensions,” *Opt. Eng.* **43**(7), 1489 (2004).
19. W. Lin et al., “Advances in the SMS design method for imaging optics,” *Proc. SPIE* **8167**, 81670M (2011).
20. J. C. Miñano et al., “Overview of the SMS design method applied to imaging optics,” *Proc. SPIE* **7429**, 74290C (2009).
21. F. Duerr et al., “Analytic free-form lens design for imaging applications with high aspect ratio,” *Proc. SPIE* **8486**, 848609 (2012).
22. R. R. Shannon, *The Art and Science of Optical Design*, Cambridge University Press, Cambridge (1997).
23. F. Duerr, Y. Meuret, and H. Thienpont, “Potential benefits of free-form optics in on-axis imaging applications with high aspect ratio,” *Opt. Express* **21**(25), 31072 (2013).
24. P. Benítez and J. C. Miñano, “Ultrahigh-numerical-aperture imaging concentrator,” *J. Opt. Soc. Am. A* **14**(8), 1988–1997 (1997).
25. F. Duerr et al., “Perfect imaging of three object points with only two analytic lens surfaces in two dimensions,” *Proc. SPIE* **8429**, 842908 (2012).
26. R. E. Fischer et al., *Optical system design*, McGraw Hill, New York (2000).
27. G. W. Forbes, “Robust, efficient computational methods for axially symmetric optical aspheres,” *Opt. Express* **18**(19), 19700–19712 (2010).
28. F. Robert, T. Biljana, and Y. Paul, “Basic optics and optical system specifications,” in *Optical System Design*, McGraw Hill Professional, Access Engineering (2008).

Yunfeng Nie received her BS degree in mechanical engineering from the University of Science and Technology of China (USTC) in 2009 and her MS degree in optical engineering from the University of Chinese Academy of Sciences (UCAS) in 2012. She is currently a PhD candidate in B-Phot team at Vrije Universiteit Brussel (VUB) in Belgium. Her research interests include optical design and imaging freeform optics. She is a member of SPIE.

Fabian Duerr graduated in physics from the Karlsruhe Institute of Technology (KIT), Germany in 2008. He then joined the Department of Applied Physics and Photonics at the Vrije Universiteit Brussel (VUB), Belgium in 2009, where he received his PhD degree in applied sciences in 2013. As a postdoctoral research fellow of FWO-Vlaanderen, he is currently responsible for a research group that explores the potential of novel free-form optical designs. He is a member of SPIE and OSA.

Hugo Thienpont graduated as an electrotechnical engineer in 1984 and received his PhD degree in applied sciences in 1990, both at the Vrije Universiteit Brussel (VUB), Belgium. In 1994, he became a professor at the Faculty of Engineering. In 2000, he became research director of the Department of Applied Physics and Photonics at the VUB, and in 2004, he was elected chair of the department. He is a fellow member of SPIE and EOS, and a member of OSA and the IEEE Photonics Society.